Three-Dimensional Visualization of the Rotavirus Hemagglutinin Structure

A. L. Shaw,* R. Rothnagel,* D. Chen,†
R. F. Ramig,† W. Chiu,*
and B. V. Venkataram Prasad*
*Verna and Marrs McLean Department of Biochemistry
and the W. M. Keck Center for Computational Biology
†Division of Molecular Virology
Baylor College of Medicine
Houston, Texas 77030

Summary

Three-dimensional structures of a native simian and reassortant rotavirus have been determined by electron cryomicroscopy and computer image processing. The structural features of the native virus confirm that the hemagglutinin spike is a dimer of VP4, substantiated by in vivo radiolabeling studies. Exchange of native VP4 with a bovine strain equivalent results in a poorly infectious reassortant. No VP4 spikes are detected in the three-dimensional reconstruction of the reassortant. The difference map between the two structures reveals a novel large globular domain of VP4 buried within the virion that interacts extensively with the intermediate shell protein, VP6. Our results suggest that assembly of VP4 precedes that of VP7, the major outer shell protein, and that VP4 may play an important role in the receptor recognition and budding process through the rough endoplasmic reticulum during virus maturation.

Introduction

Rotavirus, a genus within the virus family Reoviridae, is a leading cause of severe infantile gastroenteritis worldwide. The mature virion contains six structural proteins and 11 segments of double-stranded RNA (Kapikian and Chanock, 1990; Estes, 1990). The three-dimensional structure of rotavirus was first determined by electron cryomicroscopy and computer image processing techniques (Prasad et al., 1988). Subsequent studies provided additional evidence for the identification of topographical features of the viral structural proteins (Prasad et al., 1990; Yeager et al., 1990).

The mature rotavirion is ~ 1000 Å in diameter and exhibits T = 13 icosahedral symmetry. Rotavirus is classically described as a double-shelled virus, consisting of an inner shell composed of the major structural protein, VP6, and an outer shell composed of two structural proteins, VP4 and VP7 (Estes and Cohen, 1989). The inner shell surrounds the core, which encompasses the genome and is composed predominantly of VP2, as well as minor amounts of VP1 and VP3. Prasad and Chiu (1993), based on the radial density profile computed from the three-dimensional density map of the mature rotavirion, have proposed that rotavirus is a triple-shelled structure with an inner VP2 shell, an intermediate VP6 shell, and an outer shell of VP4 and VP7. The VP2 shell lies between the radii of 210 and 265 Å. The existence of this shell is further substantiated by self-assembly of baculovirus-expressed VP2 into shells with a radius of ~ 265 Å (Labbe et al., 1991). The knobby trimers of VP6 constitute the intermediate shell, between the radii of ~ 265 and 350 Å. The VP6 shell is bristly in appearance under the electron microscope and is perforated with 132 aqueous channels that lie on a T = 13 levo icosahedral lattice. VP7, a glycoprotein, forms a smooth outer shell of ~ 30 Å in thickness, between the radii of 350 and 380 Å. This shell contains 132 aqueous channels that are in register with those in the VP6 shell. VP4, the minor of the two outer shell proteins, forms spikes that extend ~ 120 Å from the VP7 surface. These spikes are located at one edge of the peripentonal channels and have been suggested to be dimers based on binding of two monoclonal anti-VP4 Fab fragments per spike (Prasad et al., 1990). It should be mentioned here that, consistent with the observations that rotavirus is a triple-shelled particle, we will refer to the mature particles as triple-shelled particles (previously described as double-shelled particles) and the particles that lack the outer shell as double-shelled particles (previously described as single-shelled particles).

The spike protein, VP4, has been implicated in several roles during rotavirus infection. VP4 is the rotaviral hemagglutinin (Kalica et al., 1983), is a determinant of virulence and growth in cell culture (Offit et al., 1986), and appears to be involved in cell binding (Ruggeri and Greenberg, 1991; Bass et al., 1991) and penetration (Kaljot et al., 1988). In addition, VP4 is susceptible to trypsin, resulting in the cleavage products VP5* (~ 60 kd) and VP8* (~ 28 kd). Proteolysis of VP4 significantly enhances viral infectivity (Espejo et al., 1981; Estes et al., 1981). VP4 may also play a role in the maturation of progeny rotavirions (Maass and Atkinson, 1990), in which double-shelled particles bud through the endoplasmic reticulum and become transiently enveloped prior to acquisition of the outer shell proteins (Estes, 1990).

To study the structural and functional aspects of VP4, we have exploited the ability of rotavirus to undergo reassortment. The functions of various viral proteins of the segmented genome viruses, notably of the Reoviridae (Ramig and Ward, 1991), the Orthomyxoviridae (Ritchey et al., 1976), and the Bunyaviridae (Endres et al., 1991; Endres et al., 1989), have been elucidated by examining the phenotypic and genotypic variation between reassortants and their parental strains. We have chosen for our structural studies a well-characterized simian variant, SA11-4F, and an SA11-4F reassortant, R-004. R-004 is genetically identical to SA11-4F with the exception of the VP4 genome segment, which has been exchanged for the bovine strain B223 equivalent. The exchange of VP4 results in a reassortant with significantly lowered stability and a different plaque morphology (Chen et al., 1992). In this paper, we present the structures of the native SA11-4F and the reassortant R-004, computed to ~ 28 Å resolution
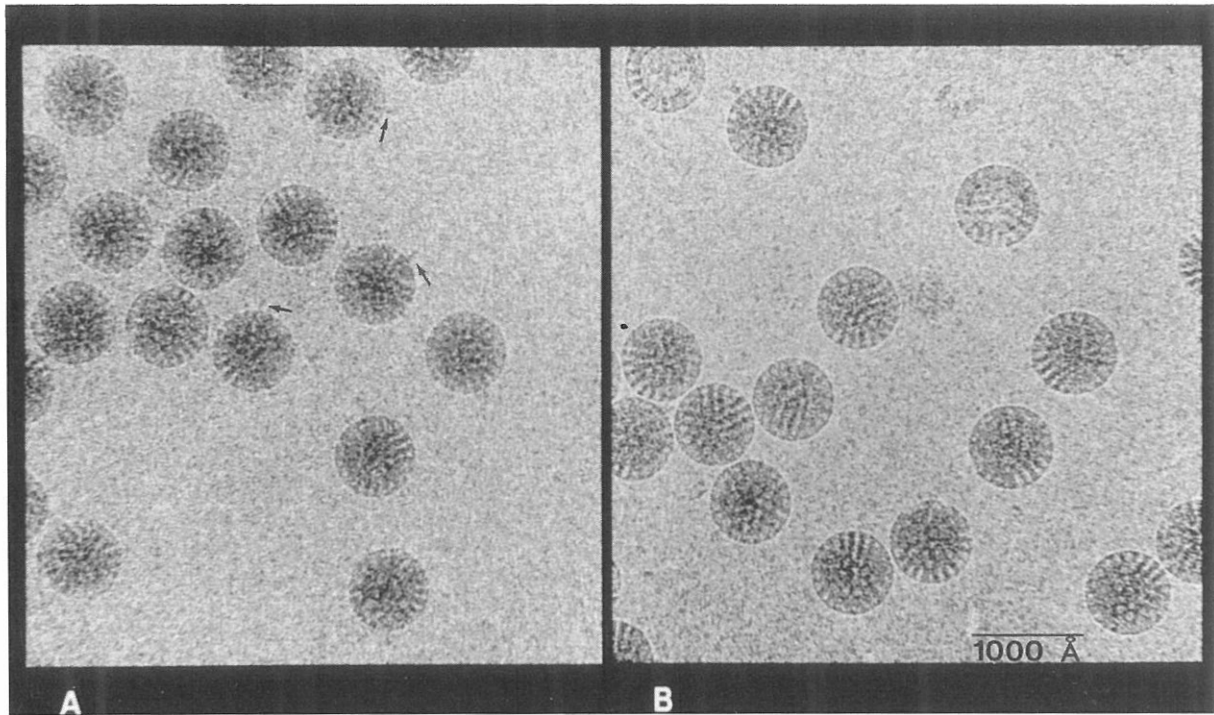
Figure 1. Cryopreservation of Native and Reassortant Rotavirus

Electron cryomicrographs of SA11-4F (A) and R-004 (B) rotavirions, embedded in a thin layer of vitreous ice, are shown. The images shown are closer to focus in the focal series. Arrows point to regions of density in SA11-4F, which correspond to the VP4 spikes. These projections are not evident in R-004.

by electron cryomicroscopy and computer image processing.

Results

Electron Cryomicroscopy

The electron cryomicrographs of SA11-4F (Figure 1A) and R-004 (Figure 1B) show the characteristic spoke-and-wheel morphology unique to rotavirus. The virions, about 765 Å in diameter excluding the spikes, exhibit a smooth outer margin. Regions of density corresponding to the VP4 spikes (indicated by arrows) project outward from the surface of several SA11-4F rotavirions. These projections are not evident in the R-004 image.

Three-Dimensional Structures of SA11-4F and R-004

The three-dimensional structures of SA11-4F and R-004 were computed from the electron cryomicrographs in Figures 1A and 1B. Because the reconstructions were computed from independent micrographs, corrections for magnification differences and for the contrast transfer function (CTF) were necessary before calculating a difference map between reconstructions (described in Experimental Procedures; see Figure 2). These corrections ascertain that the differences between the reconstructions are structural and not due to the imaging conditions. Unless otherwise mentioned, the three-dimensional structures shown are CTF corrected.
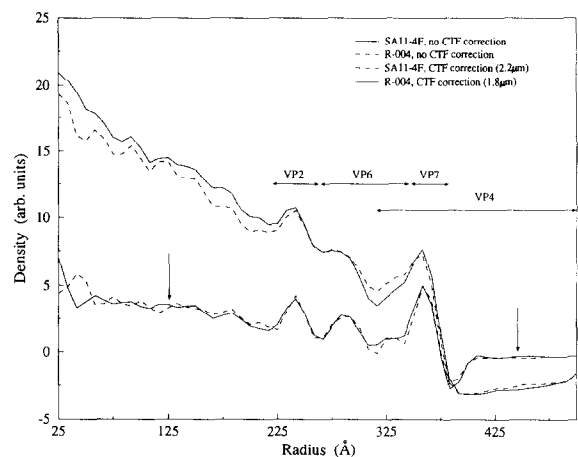
Figure 3A shows a surface representation of the

Figure 2. Radial Density Plots Computed from the Three-Dimensional Reconstruction before and after the CTF Correction

Radial density plots of the CTF-corrected reconstructions of SA11-4F (upper solid line) and R-004 (upper dashed line) and the uncorrected reconstructions of SA11-4F (lower solid line) and R-004 (lower dashed line). Arrows point to the plots without CTF corrections. The deep valley observed at ~385 Å in the plots of the uncorrected maps is due to the Fresnel fringe. The major peaks at ~360, ~290, and ~240 Å represent the VP7, VP6 and VP2 shells, respectively. The radial extensions of these shells are indicated by the double-headed arrows. Below the radius of ~200 Å, the density contributions are expected to be due to genomic RNA. A significant increase in the average density is observed below this radius only in the CTF-corrected maps, since CTF correction allows for better discrimination between the contributions from RNA and protein. A similar observation was made by Smith and Langmore (1992) on tobacco mosaic virus.
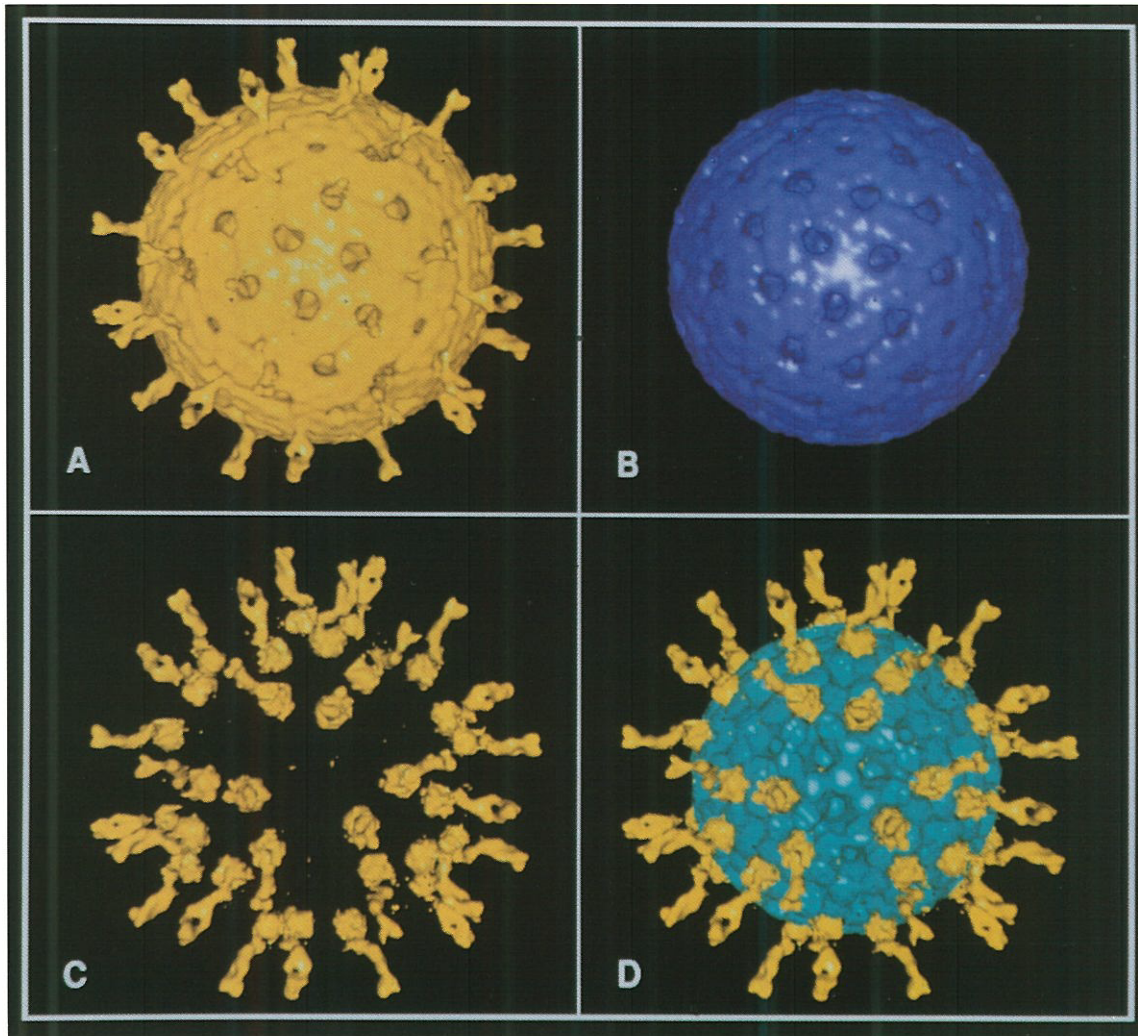
Figure 3. The VP4 Spike Extends into the Rotavirus and Interacts with the Intermediate Shell

Surface representations from the CTF-corrected three-dimensional maps are shown.

(A) The reconstructed density map of SA11-4F reveals the complex organization of the outer shell of rotavirus. The spherical shell is composed of what appear to be trimers of VP7, arranged onto a T = 13 levo icosahedral lattice. The spikes are the viral hemagglutinin and are composed of VP4. The dimeric nature of the VP4 spikes can be clearly observed from our ~28 Å resolution map.

(B) The reassortant R-004 has no VP4 spikes, which provides structural justification for the biological and biochemical distinctions between reassortant and parent (Chen and Ramig, 1992).

(C) The difference map between SA11-4F and R-004 reconstructions reveals that the VP4 spike traverses the VP7 outer shell and interacts with the VP6 inner shell.

(D) The surface representation of the R-004 VP6 shell merged with the difference map between R-004 and SA11-4F. The VP4 spikes emerge from the type II channels in the VP6 shell. The globular interior portion of VP4 covers the channel up.

SA11-4F reconstruction viewed along the icosahedral 3-fold axis, computed to ~28 Å resolution based on the phase residual criterion of the common lines (Crowther, 1971). Structural features observed in the outer surface and inside of SA11-4F are similar to those described for other strains of rotavirus (Prasad et al., 1990; Yeager et al., 1990). The surface of the VP7 outer shell is noticeably rippled, with evidence for possible trimeric clustering of the VP7 molecules. The VP7 molecules are arranged on a T = 13 levo icosahedral lattice of ~765 Å in diameter. A total of 132 aqueous channels perforate the VP7 shell at three distinct locations. Twelve type I channels are located along the icosahedral 5-fold axes. Sixty type II channels are located at the 6-coordinated positions immediately surrounding the 5-fold axes. The 60 remaining type III channels are located at the other 6-coordinated positions that neighbor the icosahedral 3-fold axes. The spikes, located at one edge of the type II channels, are ~120 Å in length from the surface of the VP7 shell. There is distinct asymmetry in the shapes of the type II and type III channel openings, while the type I channel has a circular opening. The type I channel is significantly smaller than the other two types.

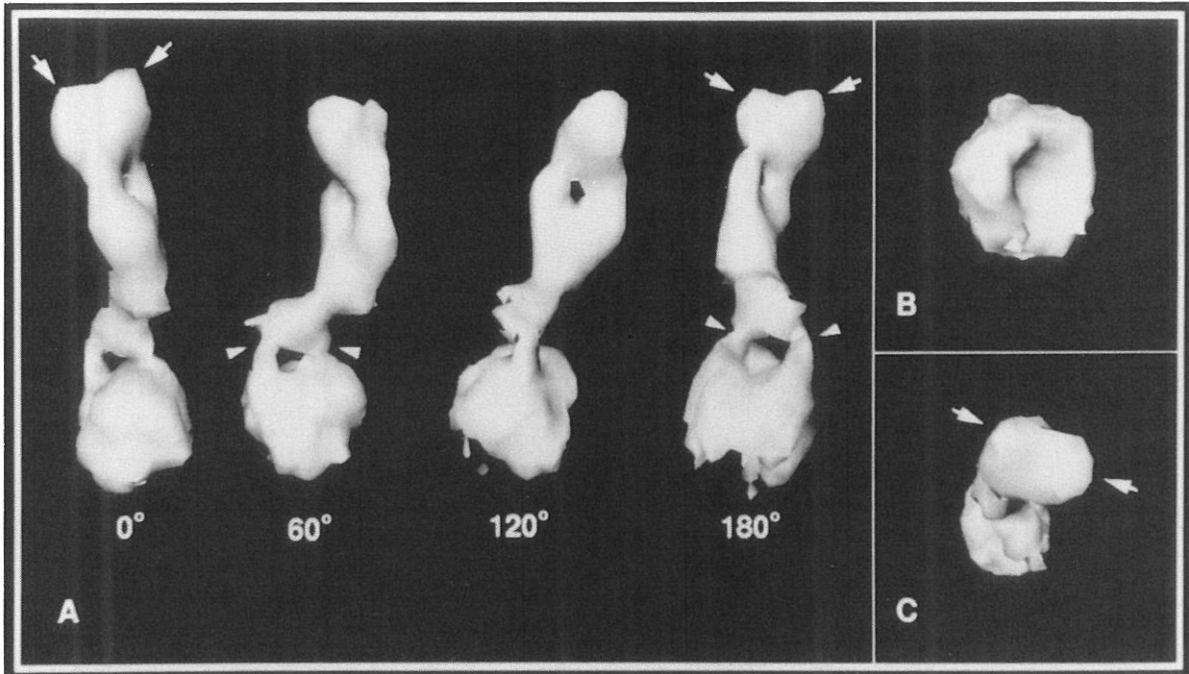Figure 3B shows the surface representation of the R-004

Figure 4. The Rotaviral Hemagglutinin Is a Dimer of VP4

(A) An isolated spike from the difference map in Figure 3C has been rotated to provide different angles for viewing. Several observations are made: two molecules of VP4 appear to participate in spike formation, and VP4 appears to form multiple contacts with VP6. The dimeric nature of the VP4 hemagglutinin is most pronounced in the exterior VP4 portion, while the globular shape of the interior portion may allow the VP4 spike to make multiple contacts with the VP6 trimers that line the type II channels. See text for an explanation of the white arrows and arrowheads.

(B) A bottom view of the VP4 spike reveals that the globular domain that lies beneath the VP7 surface is hollow in its center.

(C) A top view of the VP4 spike emphasizes the bilobed structure at its distal tip. White arrows point to the outermost edge of each lobe.

reconstruction viewed down the icosahedral 3-fold axis, also calculated to ~28 Å resolution. In comparing the R-004 and SA11-4F reconstructions, it is obvious that R-004 has no VP4 spikes. We examined the three-dimensional density maps at various contour levels and failed to detect the presence of any density that may be due to the spikes. Otherwise, the outer surface structure in the SA11-4F and R-004 reconstructions showed strong similarity in VP7 morphology.

Difference Map between SA11-4F and R-004

To discover any other structural differences apart from the obvious lack of surface spikes, particularly beneath the VP7 surface, we computed a difference map between the parent and reassortant structures. The difference map between uncorrected reconstructions (data not shown) was noisy beneath the VP7 surface and difficult to interpret. The difference map between the CTF-corrected reconstructions (Figure 3C) is significantly less noisy. A large globular mass becomes apparent that is located beneath the VP7 shell in register with each of the 60 VP4 spikes. This globular domain is associated with the exterior portion of each spike by two slender stalks. No other differences between the two structures can be detected.

To determine the relative position of the inner globular domain with respect to the VP6 inner shell, we merged a truncated map of R-004 with the difference map (Figure

3D). Density values between the radii of 325 and 533 Å in the R-004 reconstruction were removed to expose the structural organization of the VP6 inner shell. The tips of the VP6 trimers that interact with VP7 were consequently trimmed. In Figure 3D it can be seen that the spikes also extend outward from the type II channels in the VP6 inner shell, but the interior globular domains cover these channels to a large extent.

The Spike Structure

Figure 4A shows one of the 60 equivalent VP4 spikes isolated from the difference map (Figure 3C) and viewed at various angles of rotation about the longitudinal axis of the spike. We observe several recurring features in our rotation series: a bilobed structure at the distal tip of the spike (indicated by white arrows) between the radii of ~460 and 505 Å, with ~70 Å distance between the two lobes and ~40 Å width; a distinct separation in the body of the spike (120°) that widens to a maximum of ~80 Å; and two strands of density intertwining to form the spike, which associate at the base of the spike but diverge again toward the distal tip (white arrowheads). The bilobed structure of the spike is emphasized in the top view of the spike, shown in Figure 4C, where the white arrows point to the outermost edge of each lobe. The portion of the spike below the radius of 380 Å develops into a large globular
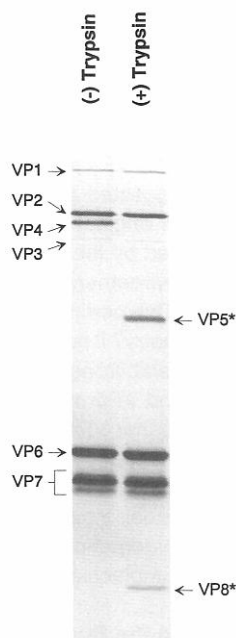
Figure 5. Autoradiogram of Uncleaved and Trypsin-Cleaved SA11-4F Proteins Labeled with [³⁵S]Methionine

Trypsin treatment of SA11-4F resulted in cleavage of VP4 into VP5* and VP8*. The well-separated bands of the trypsin treated sample were quantitated for [³⁵S]methionine content by β scan of original gels for determination of VP7:VP5* ratios.

mass seen in all of the rotational views. When viewed from the inside out, as in Figure 4B, it becomes apparent that this globular region is not a solid mass but instead is concave.

[³⁵S]Methionine In Vivo Radiolabeling Studies

To analyze the stochiometric proportions of VP4 and VP7 in the mature virion, we have carried out a ³⁵S-radiolabeling experiment. Virus was uniformly labeled with [³⁵S]methionine, digested with trypsin to cleave VP4 into VP5* and VP8*, and separated by 10% SDS–polyacrylamide gel electrophoresis (SDS–PAGE) as described in Experimental Procedures. Figure 5 shows an autoradiogram of uncleaved and trypsin-cleaved SA11-4F proteins as separated by SDS–PAGE. The radioactivity contained in VP5* and VP7 (both bands) was quantitated by β scan. Given that a virion contains 780 copies of VP7 (Prasad et al., 1988; Yeager et al., 1990), a virion contains 60 spikes, the VP5* fragment of SA11-4F VP4 contains 12 methionine residues (Mattion and Estes, 1991), and the mature form of SA11-4F VP7 contains 8 methionine residues (Stirzaker et al., 1987), the calculated VP5*:VP7 ratios would be 1:8.7, 1:4.3, and 1:2.9 if each spike contained a monomer, dimer, or trimer of VP4, respectively. The mean VP5*: VP7 ratio from four independent determinations is 1:5.0 (± 0.14 standard deviation), in good agreement with the predicted ratio for each spike consisting of two molecules of VP4.

Discussion

Heterologous Interactions Destabilize the Rotavirus Spike

The reassortant R-004, although biochemically distinct from SA11-4F, appears morphologically similar to its parent in the electron cryomicrographs. However, the three-dimensional structure of the reassortant shows no VP4 spikes. Three possibilities could explain the absence of VP4 in the R-004 structure. First, the heterologous VP4 may be unstable during assembly of the progeny virions and, during purification, become dissociated from the virus. Second, the heterologous VP4 may be present on the R-004 progeny in stoichiometric proportions but be disordered so that no VP4 structure is detected after icosahedral averaging. Third, R-004 may be assembled in vivo without any VP4. Biochemical evidence indicates that the first possibility is correct. Chen and Ramig (1992) have shown that the instability of R-004 is largely a consequence of the interactions between heterologous (B223) VP4 and native (SA11-4F) VP7. Unpurified R-004 can be neutralized by 2G4, a VP4-specific monoclonal antibody (Chen et al., 1992), suggesting that correctly folded VP4 is present on the R-004 particles. However, in the purified R-004 particles, a significantly decreased quantity of VP4 is seen by SDS–PAGE in comparison with SA11-4F. Furthermore, particle-associated VP4 decreases (along with infectivity) as storage time of the purified R-004 increases when measured by SDS–PAGE and plaque assay (D. C. and R. F. R., personal communication). Therefore, the most likely explanation for the loss of VP4 spikes from R-004 particles suggested by these results is that the heterologous VP4 becomes destabilized and falls off.

Difference Map Shows Inward Extension of the VP4 Spike

The difference map between the native and the reassortant structures reveals a large domain beneath the VP7 surface centered on the type II channel in close association with the walls of the channel made of trimers of VP6. Possible interpretations as to the identity of this globular mass include the following: first, it is the inward extension of the VP4 spike; second, it represents a conformational difference in VP6 between the native and the reassortant; or third, it is a new structural protein. The second interpretation is unlikely, since SA11-4F and R-004 are distinct only with regard to genome segment 4 and its protein, VP4. It is unlikely that the heterologous VP4 in R-004 would cause such a large conformational change in either VP6 or VP7 that they would contribute significantly to the observed globular mass. Assuming a protein density of 1.30 g/cm³, the mass of the globular feature is about 60 kd. Such significant mass displacement in VP6 between the native and the reassortant structures is improbable. Furthermore, examination of the VP6 shell in the two structures shows no evidence of mass translocation in R-004. The third interpretation also is unlikely, as there is no evidence for a new structural protein by SDS–PAGE. The observed globular mass is clearly seen connected to the

exterior of the VP4 spike. The difference between the two structures is localized only to this region, and the differences elsewhere are insignificant. Therefore, the most plausible interpretation is the first interpretation, that is, that the large globular mass is a part of the VP4 spike.

The Rotaviral Hemagglutinin Is a Dimer

The structural details in the SA11-4F reconstruction strongly indicate that the rotavirus hemagglutinin is a dimer of VP4. Mass density calculations computed from the difference map are in complete agreement with 120 molecules of VP4 (assuming molecular mass is 88 kd). The dimeric state of the VP4 spike was initially suggested by Prasad et al. (1990) from a low resolution (~35 Å) structure of the simian rotavirus strain SA11 (clone 3) complexed with anti-VP4 Fab fragments. These studies revealed two Fab molecules bound to the bilobed structure of each spike. Subsequent structural studies of Yeager et al. (1990), at ~37 Å, also pointed out the bilobed feature of the spikes in another strain of rotavirus. These authors noted the discrepancies between the structural and biochemical results pertaining to the oligomeric state of VP4 and suggested the need for more experimental evidence. The dimeric nature of the VP4 spike is evident at the present resolution of 28 Å. At this resolution, a large separation in the body of the spike is apparent, as well as the intertwining of the two strands of VP4. These features were not observed in previous reconstructions of rotavirus.

The results of previous biochemical studies are not in agreement with any oligomeric structure for the VP4 spike. Densitometric measurements from Coomassie-stained polyacrylamide gels of SA11 (Liu et al., 1988) predict a VP4:VP7 ratio of 1:55. This ratio is much lower than that predicted for even a monomeric VP4 spike (1:13). Since Coomassie blue is known to stain protein differentially, it is difficult to use this method for quantitation. Our radiolabeling studies provide a more accurate measurement of the quantity of VP4 and VP7 in the mature rotavirion. The VP5*:VP7 ratio that we have determined from highly purified [^{35}S]methionine-radiolabeled virus is in excellent agreement with each spike being a dimer of VP4.

It is not surprising that the rotavirus hemagglutinin is a VP4 dimer. Viral hemagglutinins tend to function as multimeric structures. Within the Reoviridae, the reovirus hemagglutinin, σ1 (Weiner et al., 1978; Yeung et al., 1987), has been suggested to be a trimer (Leone et al., 1991; Strong et al., 1991) or tetramer (Bassel-Duby et al., 1987; Nibert et al., 1990; Fraser et al., 1990). The σ1 protein modulates tissue tropism (Lee et al., 1981) and is functionally similar to the rotavirus VP4. Several more examples of multimeric hemagglutinins can be found in other virus families. The hemagglutinin of coronavirus, also an enteric virus, functions as a dimer (Hogue et al., 1989). The well-studied influenza hemagglutinin is a trimer (Wiley and Skehel, 1987). In addition, the hemagglutinin–neuraminidase of Sendai virus, a member of the paramyxoviridae, has been isolated in both dimeric and tetrameric forms (Laver et al., 1989).

In the VP4 spike, any 2-fold axis of symmetry is not particularly evident. The location of the spike does not correspond to any local or strict 2-fold axis of the icosahedron. Thus, the dimeric configuration is apparently asymmetric. The asymmetry of the spike can be seen clearly in the views provided by Figure 4A. This result is consistent with the result of Prasad et al. (1990), in which the two Fab fragments bound to the VP4 spike at different angles. Prasad et al. (1990) suggested that the Fab fragments exhibited different elbow angles. It is very likely that the antigenic sites recognized by the Fab fragments are not in structurally similar environments, resulting in different angles for Fab binding. One pertinent question is, to what advantage is this asymmetry? It is possible that the asymmetry is required for stabilizing interactions between quasi-equivalent VP7 and VP6 molecules. On the outer virion surface it appears that VP4 interacts with 2 molecules of VP7, but inside it appears that the large globular domain interacts with all six of the VP6 molecules surrounding the type II channel. However, it is possible that there are more specific interactions between the VP4 dimer and 2 of the 6 VP6 molecules.

Possible Role of VP4 in the Budding of Double-Shelled Virions

The presence of a large globular domain internal to the outer shell raises interesting questions regarding the assembly of VP4 in the rotavirus particles. During progeny maturation, newly assembled double-shelled particles migrate from the viroplasm to the rough endoplasmic reticulum, through which they bud, resulting in a transiently enveloped particle (Estes et al., 1983). The steps by which double-shelled particles become triple-shelled are poorly understood. One pending question is, at what stage does VP4 assembly take place, before or after the assembly of VP7? Our results favor the hypothesis that VP4 assembly precedes that of VP7 and, thus, the budding event. It would be difficult for the VP4 internal domain, which is ~70 Å in diameter, to be incorporated into the rotavirion through the VP7 type II channels, which are only ~55 Å in diameter. VP4 is synthesized on the free ribosomes in the cytoplasm (Estes, 1990). Examining Figure 3D, one can envision newly synthesized VP4 interacting with the VP6 of double-shelled particles prior to interaction with the rough endoplasmic reticulum membrane. Once assembled on the double-shelled particles, VP4 may aid in recognition of NS28, a nonstructural protein that has been implicated in mediating passage of double-shelled particles through the rough endoplasmic reticulum (Au et al., 1988). Maass and Atkinson (1990) reported the interaction of NS28 with VP4 and VP7 in infected cells. More recent evidence indicates that the cytoplasmic C-terminus of NS28 has a binding site for both single-shelled particles and VP4 (Au et al., 1993). Structural studies on double-shelled particles complexed with NS28 and VP4 will be of interest in this regard.

Conclusions

We conclude from our structural and biochemical studies that the rotavirus hemagglutinin is a dimer of VP4. The dimeric nature of the VP4 hemagglutinin can clearly be seen in our SA11-4F structure. Radiolabeling studies fur-

ther support this conclusion. We also have found that the VP4 structure traverses the outer VP7 shell and interacts with the intermediate shell protein, VP6. The difference map between SA11-4F and the reassortant R-004 reveals a large globular domain beneath the VP7 shell that is part of the VP4 structure. This result suggests that VP4 assembly occurs prior to VP7 assembly and that VP4 might interact with double-shelled particles before budding through the rough endoplasmic reticulum. Future structural studies focusing on double-shelled particles complexed with VP4 should provide better insight into the maturation process of rotavirus.

Experimental Procedures

Preparation and Purification of Native and Reassortant Virus

Two rotavirus strains were used in these studies: the first, SA11-4F, is a variant of the simian rotavirus SA11. SA11-4F was originally isolated by Pereira et al. (1984) and was extensively characterized by Burns et al. (1989). It has been shown to be more stable than the standard SA11 and is purified at higher yields (Chen and Ramig, 1992). Because of these qualities, we have chosen this variant for our structural studies. The second, reassortant virus R-004, was derived from a cross of SA11-4F and the bovine rotavirus B223. R-004 contains all SA11-4F genome segments except segment 4. Genome segment 4 and its encoded VP4 are derived from B223 in R-004 (Chen et al., 1989). In contrast with SA11-4F, R-004 is very unstable and can be purified only to low yield (Chen and Ramig, 1992). In addition, R-004 has been shown to express an unexpected antigenic phenotype (Chen et al., 1992).

Viruses were purified as previously described (Chen and Ramig, 1992). In brief, MA104 cell monolayers in 150 cm² flasks were infected with second passage virus at a multiplicity of infection of 10 pfu per cell. After 1 hr of adsorption at 37°C, the inoculum was removed, and the infected monolayer was maintained in 20 ml of serum-free medium 199 containing 1% aprotinin (Sigma; 22 U/ml). The infected monolayer was incubated at 37°C until complete cytopathic effect was observed. Cell lysates were frozen and thawed three times before purification by a standard CsCl gradient protocol. The triple-shelled particles were collected and dialyzed extensively against Tris-buffered saline (8.0 g/l NaCl, 0.38 g/l KCl, 0.1 g/l Na₂HPO₄, 1.0 g/l dextrose, 3.0 g/l Tris, 0.1 g/l MgCl₂, 0.1 g/l CaCl₂ [pH 7.4]) at 4°C. Triple-shelled particles were stored at 4°C in the presence of 0.01% NaN₃.

Preparation of [³⁵S]Methionine-Labeled Virus

Radiolabeled virus was prepared as follows: MA104 cell monolayers in 150 cm² flasks were infected with 20 pfu per cell of SA11-4F. Flasks were incubated for 1 hr at 37°C to allow virus adsorption to cells, and the inoculum was removed. The infected monolayer then was maintained in 20 ml of Eagle's medium lacking methionine for 2.5 hr at 37°C. The monolayer then was put in 20 ml of Eagle's medium lacking methionine per 150 cm² flask, to which 20 mCi/ml of [³⁵S]methionine (ICN, 1029 Ci/mmole) and 5 mg/ml of actinomycin D were added. The flasks were incubated at 37°C until complete cytopathic effects were observed. Virus was purified by standard CsCl gradient methods as previously described (Chen and Ramig, 1992). Purified triple-shelled particles were suspended in Tris-buffered saline and stored at 4°C in the presence of 0.01% NaN₃.

Quantitation of Relative Ratio of Radiolabeled VP7:VP5*

Direct quantitation of VP4 by SDS–PAGE is difficult because VP4 migrates closely to VP2. However, the VP4 trypsin cleavage products, VP5* and VP8*, do not migrate closely to any rotaviral proteins. Virus particles were treated with 5 μg/ml trypsin before SDS–PAGE analysis. The radioactivity of VP5* and VP7 was measured by quantitation of counts per minute (cpm) in bands separated by 10% SDS–PAGE using a betascope blot analyzer (Model 603, Betagen, Waltham, Massachusetts).

Electron Cryomicroscopy

Specimen preparation for electron cryomicroscopy is well established (Dubochet et al., 1988; Prasad et al., 1992). We have employed a containment system adapted for virus specimen preparation (Jeng et al., 1988). The virus suspension (~5 μl) was placed onto a carbon-coated holey grid, blotted, and plunged into a bath of liquid ethane (-180°C). The frozen-hydrated specimen was transferred under liquid nitrogen to a GATAN cryoholder and observed in a JEOL 1200 transmission electron microscope at 100 kV and a specimen temperature of −165°C. Micrographs with regions of interest were recorded as focal pairs with intended sequential underfocus settings of −1 μm and ~2 μm, using low electron dose of ~5 e⁻/Å² with a nominal magnification of 30,000 x.

Computer Image Processing

Micrographs were digitized using a Perkin-Elmer Micro-10 microdensitometer with a step size of 25 μm² per pixel, which corresponds to 8.33 Å in the object. Individual particles were boxed into a 128 × 128 pixel region, floated, and masked with a suitable radius. The three-dimensional reconstruction procedure is similar to that used in earlier studies (Crowther, 1971; Fuller, 1987; Baker et al., 1990; Prasad et al., 1992, 1993). Both SA11-4F and R-004 reconstructions were generated by particles chosen from a single micrograph. The center of each particle (corresponding to the phase origin) was determined using cross-correlation methods. The orientation of each particle was determined by a common lines procedure (Crowther, 1971; Fuller, 1987), which makes use of the icosahedral symmetry. Particles in the image further from focus, which exhibits enhanced contrast, were used to find the orientations of the corresponding particles in the image closer to focus. The images closer to focus were used for the three-dimensional reconstruction. Only those orientations that gave rise to a phase residual value of less than 50° were considered for the reconstruction. The phase origins and orientations were refined iteratively using intra- and interparticle refinement methods. Once a well-distributed set of particles was established (~40 particles), the three-dimensional density map was generated using cylindrical expansion. The reconstructions were computed to a resolution of ~28 Å, as judged by the phase residual values. Surface representations of the three-dimensional maps were generated and displayed with IRIS Explorer (Silicon Graphics; 1991).

Corrections for Magnification Differences and the CTF

Since the two structures were obtained from two different micrographs, it was necessary to correct for the possible differences in magnification and defocus levels prior to computing the difference map. Two steps were carried out before computing the difference map between native and reassortant structures. In the first step, particles were scaled in Fourier space to account for the possible magnification differences between the two micrographs. The appropriate radial scale factor was computed by calculating the average phase residual for the 60 cross common lines in a pairwise comparison of the particles, using one particle from the SA11-4F set as a template. The radial scale factor was varied between 0.85 and 1.15 at an interval of 0.01, and the phase residual for the cross common lines was computed as a function of the radial scale factor. The magnification difference between the micrographs was determined to be ~0.8%.

In the second step, the amplitudes in the Fourier transforms of the particles were corrected for the CTF (Erickson and Klug, 1971), using an amplitude contrast factor, or Q value, of 14% of the phase contrast (Smith and Langmore, 1992). This factor was previously estimated to be about 7% by Toyoshima and Unwin (1988). Smith and Langmore (1992) have suggested that their estimation of 14% could be due to thicker ice. To embed the virus particles completely, the ice thickness has to be more than 1000 Å. Hence, we chose the value of 14%. Since the reconstructions were carried out to a resolution lower than that corresponding to the first minimum of CTF, no corrections to phases were necessary.

To calculate the CTF, the precise defocus value must be known. To calculate the value of defocus we made use of the Fresnel fringe (white ring) that is seen gracing the periphery of the particle images. The Fresnel fringes arise owing to the interference between the scattered and unscattered electrons. In focus, the particle edge, representing a sharp discontinuity in the object, has low contrast, and the Fresnel

fringe is not perceptible. When defocused, these fringes are clearly seen, and their width is directly proportional to the level of defocus (Hall, 1966). The Fresnel fringe manifests itself as a deep valley at a radius corresponding to the outer surface in the radial density plot computed from the three-dimensional density maps (Figure 2). We varied the defocus value between 0.5 μm and 2.5 μm with an initial interval of 0.2 μm to determine a rough estimate of the defocus value, and later an interval of 0.1 μm to refine our estimate. For each defocus value within the range specified above, the amplitudes in the particles within the first minimum were corrected for the CTF, using C_s value of 5.4 mm and a Q value of 14%. The three-dimensional reconstruction was computed using these corrected amplitudes. A radial density plot was then generated, following the procedure described in Prasad et al. (1993), from the CTF-corrected reconstructions and examined to see if the minimum from the Fresnel fringe had flattened. Using the disappearance of the minimum in the radial density plots as an indicator, the appropriate defocus value for each reconstruction was determined. This minimum flattens out for SA11-4F when using a defocus value of 2.2 μm and for R-004 when using a defocus value of 1.8 μm. For confirmation, we also calculated the defocus value of the corresponding micrograph of the focal pair of SA11-4F, which is 1 μm further from focus, and found the defocus value to be 3.2 μm. The evaluation of the defocus values using the Fresnel fringe is possible only because of the relatively smooth outer surface of the rotavirus particles.

Acknowledgments

References

Au, K. S., Chan, W. K., and Estes, M. K. (1988). Rotavirus morphogenesis involves an endoplasmic reticulum transmembrane glycoprotein. UCLA Symp. Mol. Cell. Biol. 90, 257–267.

Au, K.-S., Mattion, N. M., and Estes, M. K. (1993). A subviral particle binding domain on the rotavirus nonstructural glycoprotein NS28. Virology 194, 665–673.

Baker, T. S., Newcomb, W. W., Booy, F. P., Brown, J. C., and Stevern, A. C. (1990). Three-dimensional structures of maturable and abortive capsids of equine herpesvirus 1 from cryoelectron microscopy. J. Virol. 64, 563–573.

Bass, D. M., Mackow, E. R., and Greenberg, H. B. (1991). Identification and partial characterization of a rhesus rotavirus binding glycoprotein on murine enterocytes. Virology 183, 602–610.

Bassel-Duby, R., Nibert, M. K., Homcy, C. J., Fields, B. N., and Sawutz, D. G. (1987). Evidence that the sigma 1 protein of reovirus serotype 3 is a multimer. J. Virol. 61, 1834–1841.

Burns, J. W., Chen, D., Estes, M. K., and Ramig, R. F. (1989). Biological and immunological characterization of a simian rotavirus SA11 variant with an altered genome segment 4. Virology 169, 427–435.

Chen, D., Burns, J. W., Estes, M. K., and Ramig, R. F. (1989). Phenotypes of rotavirus reassortants depend upon the recipient genetic background. Proc. Natl. Acad. Sci. USA 86, 3743–3747.

Chen, D., Estes, M. K., and Ramig, R. F. (1992). Specific interactions between rotavirus outer capsid proteins VP4 and VP7 determine expression of a cross-reactive, neutralizing VP4-specific epitope. J. Virol. 66, 432–439.

Chen, D. Y., and Ramig, R. F. (1992). Determinants of rotavirus stability and density during CsCl purification. Virology 186, 228–237.

Crowther, R. A. (1971). Procedures for three-dimensional reconstruction of spherical viruses by Fourier synthesis from electron micrographs. Phil. Trans. R. Soc. Lond. (B) 261, 221–230.

Dubochet, J., Adrian, M., Chang, J. J., Homo, J. C., Lepault, J., McDowall, A. W., and Schultz, P. (1988). Cryo-electron microscopy of vitrified

specimens. Quart. Rev. Biophys. 21, 129–228.

Endres, M. J., Jacoby, J. R., Janssen, R. S., Gonzalez-Scarano, F., and Nathanson, N. (1989). The large viral RNA segment of California serogroup bunyaviruses encodes the large viral protein. J. Gen. Virol. 70, 223–228.

Endres, M. J., Griot, C., Gonzalez-Scarano, F., and Nathanson, N. (1991). Neuroattenuation of an avirulent bunyavirus variant maps to the L RNA segment. J. Virol. 65, 5465–5470.

Erickson, H. P., and Klug, A. (1971). The Fourier transform of an electron micrograph: effects of defocussing and aberrations, and implications for the use of underfocus contrast enhancement. Phil. Trans. R. Soc. Lond. (B) 261, 105–118.

Espejo, R. T., Lopez, S., and Arias, C. F. (1981). Structural polypeptides of simian rotavirus SA11 and the effect of trypsin. J. Virol. 37, 156–160.

Estes, M. K. (1990). Rotaviruses and their replication. In Virology, B. N. Fields, ed. (New York: Raven Press), pp. 1329–1352.

Estes, M. K., and Cohen, J. (1989). Rotavirus gene structure and function. Microbiol. Rev. 53, 410–449.

Estes, M. K., Graham, D. Y., and Mason, B. B. (1981). Proteolytic enhancement of rotavirus infectivity molecular mechanisms. J. Virol. 39, 879–888.

Estes, M. K., Palmer, E. L., and Obijeski, J. F. (1983). Rotaviruses: a review. Curr. Topics Microbiol. Immunol. 105, 123–184.

Fraser, R. D., Furlong, D. B., Trus, B. L., Nibert, M. L., Fields, B. N., and Stevens, A. C. (1990). Molecular structure of the cell attachment protein of reovirus correlation of computer-processed electron micrographs with sequence-based predictions. J. Virol. 64, 2990–3000.

Fuller, S. D. (1987). The T = 4 envelope of Sindbis virus is organized by interactions with a complementary T = 3 capsid. Cell 48, 923–934.

Hall, C. E. (1966). Introduction to Electron Microscopy (New York: McGraw Hill).

Hirst, G. K. (1962). Genetic recombination with Newcastle disease virus, poliovirus, and influenza virus. Cold Spring Harbor Symp. Quant. Biol. 27, 303–308.

Hogue, B. G., Kienzle, T. E., and Brian, D. A. (1989). Synthesis and processing of the bovine enteric coronavirus hemagglutinin protein. J. Gen. Virol. 70, 345–352.

Jeng, T. W., Talmon, Y., and Chiu, W. (1988). Containment system for the preparation of vitrified-hydrated virus specimens. J. Electron Microsc. Tech. 8, 343–348.

Kalica, A. R., Flores, J., and Greenberg, H. B. (1983). Identification of the rotaviral gene that codes for the hemagglutinin and protease-enhanced plaque formation. Virology 125, 194–205.

Kaljot, K. T., Shaw, R. D., Rubin, D. H., and Greenberg, H. B. (1988). Infectious rotavirus enters cells by direct cell membrane penetration, not by endocytosis. J. Virol. 62, 1136–1144.

Kapikian, A. Z., and Chanock, R. M. (1990). Rotaviruses. In Virology, B. N. Fields, ed. (New York: Raven Press), pp. 1353–1404.

Labbe, M., Charpilenne, A., Crawford, S. E., Estes, M. K., and Cohen, J. (1991). Expression of rotavirus VP2 produces empty corelike particles. J. Virol. 65, 2946–2952.

Laver, W. G., Thompson, S. D., Murti, K. G., and Portner, A. (1989). Crystallization of Sendai virus HN protein complexed with monoclonal antibody Fab fragments. Virology 171, 291–293.

Lee, P. W. K., Hayes, E. C., and Joklik, W. K. (1981). Protein sigma 1 is the reovirus cell attachment protein. Virology 108, 156–163.

Leone, G., Duncan, R., and Lee, P. W. (1991). Trimerization of the reovirus cell attachment protein (sigma 1) induces conformational changes in sigma 1 necessary for its cell-binding function. Virology 184, 758–761.

Liu, M., Offit, P. A., and Estes, M. K. (1988). Identification of the simian rotavirus SA11 genome segment 3 product. Virology 163, 26–32.

Maass, D. R., and Atkinson, P. H. (1990). Rotavirus proteins VP7, NS28, and VP4 form oligomeric strucutres. J. Virol. 64, 2632–2641.

Mattion, N. M. and Estes, M. K. (1991). Sequence of a rotavirus gene 4 associated with unique biological properties. Arch. Virol. 120, 109–113.

Nibert, M. L., Dermody, T. S., and Fields, B. N. (1990). Structure of the reovirus cell-attachment protein a model for the domain organization of sigma 1. J. Virol. 64, 2976–2989.

Offit, P., Blavat, G., Greenberg, H. B., and Clark, H. F. (1986). Molecular basis of rotavirus virulence role of gene segment 4. J. Virol. 57, 46–49.

Pereira, H. G., Azeredo, R. S., Fialho, A. M., and Vidal, M. N. P. (1984). Genomic heterogeneity of simian rotavirus SA11. J. Gen. Virol. 65, 815–818.

Prasad, B. V. V., and Chiu, W. (1993). Structure of rotavirus. Curr. Topics Microbiol. Immunol., in press.

Prasad, B. V. V., Wang, G. J., Clerx, J. P. M., and Chiu, W. (1988). Three-dimensional structure of rotavirus. J. Mol. Biol. 199, 269–275.

Prasad, B. V. V., Burns, J. W., Marietta, E., Estes, M. K., and Chiu, W. (1990). Localization of VP4 neutralization sites in rotavirus by three-dimensional cryo-electron microscopy. Nature 343, 476–479.

Prasad, B. V. V., Yamaguchi, S., and Roy, P. (1992). Three-dimensional structure of single-shelled bluetongue virus. J. Virol. 66, 2135–2142.

Prasad, B. V. V., Prevelige, P. E., Marietta, E., Chen, R. O., Thomas, D., King, J., and Chiu, W. (1993). Three-dimensional transformation of capsids associated with genome packaging in a bacterial virus. J. Mol. Biol. 231, 65–74.

Ramig, R. F., and Ward, R. L. (1991). Genomic segment reassortment in rotavirus and other Reoviridae. Adv. Virus Res. 39, 164–207.

Ritchey, M. B., Palese, P., and Schulman, J. L. (1976). Mapping of the influenza virus genome. III. Identification of genes coding for nucleoprotein, membrane protein, and nonstructural protein. J. Virol. 20, 307–313.

Ruggeri, F. M., and Greenberg, H. B. (1991). Antibodies to the trypsin cleavage peptide VP8 neutralize rotavirus by inhibiting binding of virions to target cells in culture. J. Virol. 65, 2211–2219.

Smith, M. F., and Langmore, J. P. (1992). Quantitation of molecular densities by cryo-electron microscopy. J. Mol. Biol. 226, 763–774.

Stirzaker, S. C., Whitfield, P. L., Christie, D. L., Bellamy, A. R., and Both, G. W. (1987). Processing of rotavirus glycoprotein VP7: implications for the retention of the protein in the endoplasmic reticulum. J. Cell Biol. 105, 2897–2903.

Strong, J. E., Leone, G., Duncan, R., Sharma, R. K., and Lee, P. W. (1991). Biochemical and biophysical characterization of the reovirus cell attachment protein sigma 1: evidence that it is a homotrimer. Virology 184, 23–32.

Toyoshima, C., and Unwin, P. N. T. (1988). Contrast transfer for frozen-hydrated specimens: determination from pairs of defocused images. Ultramicroscopy 25, 279–291.

Weiner, H. L., Ramig, R. F., Mustoe, T. A., and Fields, B. N. (1978). Identification of the gene coding for the hemagglutinin of reovirus. Virology 86, 581–584.

Wiley, D. C., and Skehel, J. J. (1987). The structure and function of the hemagglutinin membrane glycoprotein of influenza virus. Annu. Rev. Biochem. 56, 365–394.

Yeager, M., Dryden, K. A., Olson, N. H., Greenberg, H. B., and Baker, T. S. (1990). Three-dimensional structure of rhesus rotavirus by cryo-electron microscopy and image reconstruction. J. Cell Biol. 110, 2133–2144.

Yeung, M. C., Gill, M. J., Alibhai, S. S., Shahrabadi, M. S., and Lee, P. W. K. (1987). Purification and characterization of the reovirus cell attachment protein sigma 1. Virology 156, 377–385.